Accurately positioning events in a high-resolution PET system that uses 3D CZT detectors

Guillem Pratx, *Member, IEEE,* Craig S. Levin, *Member, IEEE*

I. Introduction

We are investigating the use of Cadmium-Zinc-Telluride (CZT) [1] for high-resolution PET. CZT has very good energy and spatial resolution, but suffers from poor timing resolution. Furthermore as a low Z material, the photo-fraction is low and multiple interactions in the detectors are frequent [2]. However, the 3-D position of individual interactions can be read out from the detector.

The position assigned to each incoming photon needs to be estimated from the set of interactions it has created. The ideal event position is the first interaction, because it best defines the correct line of response (LOR) along which the two annihilation photons traveled. Subsequent interactions after the first one are useful for measuring the total energy of the event. Since the time of each interaction is not known with sufficient accuracy to determine which interaction happened first, we are investigating positioning methods that rely on the two other measured quantities: energy and position.

For the purpose of image reconstruction, an estimate for the first interaction is sufficient. However, it is also desirable for other applications (such as Compton PET [3], random correction [4]) to sequence the secondary interactions as well.

We first compare six basic event positioning algorithms, and then investigate the potential improvement of using a more advanced estimation technique based on the kinematics of Compton scatter.

II. Methods

A. Pre-clinical PET system based on CZT detectors.

We are developing a small-animal PET system [1] based on cross-strip edge-on CZT detectors. In this set-up, 511 keV photons traverse a minimum of 4 cm thick CZT for high photon detection efficiency. The tangential coordinate of a photon interaction is given by a pattern of 1mm-spaced anodes, the axial coordinate by the ratio between the cathode and anode digitized pulse heights, and the depth coordinate is given by a pattern of 5mm-spaced cathodes. The accuracy of event positioning algorithms can be affected by the limited energy and spatial resolution, however CZT detectors provide both high energy (¡3% at 511 keV) and spatial (1x5x1 mm) resolution to help mitigate these effects. The detectors are arranged in a box-shaped geometry, 4 cm thick, with inner dimensions of 8x8x8 cm (Fig. 1(a)).

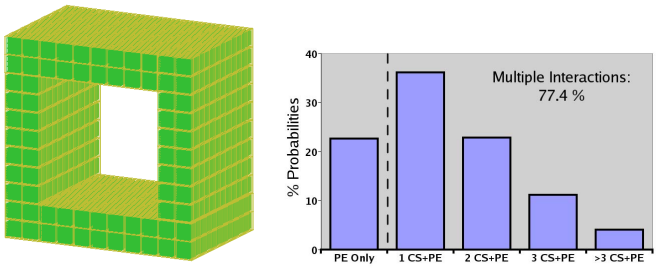

(a) (b)

Fig. 1. (a) Small-animal PET system based on 1-mm resolution CZT detectors with $8x8x8cm^3$ box-shaped FOV. (b)Distribution of the number of interactions in CZT for events that were fully absorbed. PE: Photoelectric CS: Compton scatter.

The frequency of single photons generating multiple interactions in CZT was evaluated using Monte-Carlo simulations {citeLE04.3, and is presented in Figure 1(b). Multiple interactions occur for 77.4% of the events detected within the energy window, with an average of 2.3 interactions per event, motivating the development of special algorithms to estimate the best position for such events.

The Monte-Carlo package GATE was used to simulate the system. Consistent with measurements [1], we modeled the energy resolution by adding Gaussian noise whose FWHM is $3\% * \sqrt{511/E}$, where E is the energy of the single interaction in keV. To keep the simulation as realistic as possible, the output from the GATE hits file was used to position each photon event. It was assumed that forming clusters with the interactions belonging to the same event is possible and error free. Each interaction was binned to the center of the nearest 1x1x5 mm detector voxel to simulate realistic detector resolution.

B. Basic positioning algorithms

In this work, we first looked at six simple positioning algorithms. The minimum time algorithm, where time is known perfectly, was implemented as a gold standard. Weighted mean, the only available algorithm for conventional PET block detectors, was implemented for reference; a non-weighted position average as well as location of minimum and maximum energy

This work was supported by the National Institutes of Health (NIH) under grants R01CA119056, R33EB003283, R01CA120474; by the California Breast Cancer Research Program under grant 12IB-0092; by the Stanford Bio-X program and by NVIDIA Corporation.

*G. Pratx is with Stanford University, Departments of Electrical Engineering, Radiology, and Molecular Imaging Program at Stanford. (email:pratx@stanford.edu)

CS Levin is with Departments of Radiology, Bioengineering, and the Molecular Imaging Program at Stanford.

deposited algorithms were also investigated. Finally, the minimum distance algorithm selects the first interaction based on the distance traversed in the crystal. In this scheme, weighted mean is first applied to estimate the rough location for each photon in a paired coincident event, then the particular interaction within each photon cluster that minimizes the distance with the other coincident photon pair is selected as the 'first' interaction. The intuition behind this scheme is that incoming photons are exponentially attenuated with distance into the detector and Compton scattering for annihilation photon energies are most likely forward scattering, making it likely that the interaction closest to the emission location is the first one. This statement can be empirically verified. This scheme fails when the first interaction is a large angle scatter, suggesting that improvement can be obtained by combining both energy and spatial information to retrace the sequence of events.

C. Maximum-likelihood formulation

We have also implemented a maximum-likelihood formulation for the first interaction estimation problem. The first interaction is indirectly found by estimating which sequence of interactions is most likely. For such a problem, we found that the likelihood function is complex and does not have a closed-form expression. We have therefore used Monte-Carlo integration to compute the likelihood of sequences. We used the Compton scatter formula

$$E_2 = \frac{E_1}{\frac{E_1}{m_e c^2}(1 - cos\theta) + 1} \tag{1}$$

to determine which sequences were inconsistent with the measured energies. In this equation, E_1 is the incoming photon energy, E_2 is the energy of the photon after the Compton process, θ is the scatter angle and $m_e c^2 = 511keV$ is the product of the mass of the electron times the speed of light squared.

Implementation: For a coincident pair comprising two 511 keV events, interactions were assumed to have been correctly grouped in two clusters. For a given cluster containing N detector hits, there are $N!$ possible sequences. The likelihood is evaluated for each of the $N!$ sequences and the one with maximal likelihood is chosen. In this work, the likelihood is formulated as

$$L(\sigma) = P(E_m = E_c(S)|S = \sigma) \tag{2}$$

where σ is the discrete parameter representing a test sequence; E_m is a random vector describing the statistical distribution of the energy deposited in each detector as predicted by the measurements; $E_c(S)$ is a random vector describing the statistical distribution of each energy deposited in each detector as computed from the kinematics of Compton scatter, assuming that the sequence S happened. Note that for infinitely small crystals (perfect spatial resolution), $E_m(S)$ would be simply determined from the Compton scatter formula. But for realistic detectors, the uncertainty on the position within the crystal translates into an uncertainty on the scatter angle that in turn creates uncertainty in the energy deposited in the detector by Compton scatter. While E_m follows a normal distribution centered on the measured energy e_m, $E_c(S)$ is more complex and needs to be computed by Monte-Carlo methods for each sequence S.

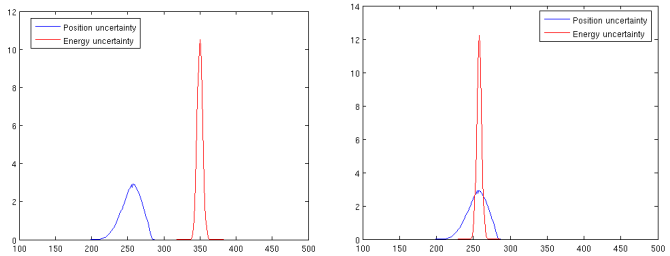

(a) (b)

Fig. 2. (a) Compton scatter interaction inconsistent with measurements (b) Compton scatter interaction consistent with measurements

This is accomplished by generating a set of uniformly distributed locations in each detector, and for each sequence of locations the scatter angle and the deposited energy are computed. Energies are then histogrammed to create an estimate of the statistical distribution for $E_c(S)$. The likelihood function is also computed for each sequence S.

Figure 2 shows the probability density function for E_m (blue) and $E_c(S)$ (red). Consistent sequences will lead to the blue curve and the red curve having a large overlap (Fig. 2(b)). The likelihood is the integral of the product of the two curves. An optimization to this method that we have implemented is that instead of computing the complete likelihood for each sequence, we look independently at each component which allows us to rule out inconsistent sequences without having to examine the full likelihood of these sequences. The resulting likelihood can be approximated as

$$L(\sigma) \approx L(CS_1, \sigma) \ldots . L(CS_N, \sigma) L(PE, \sigma) \tag{3}$$

This expression is approximate because the random vector $E_c(S)$ components are not completely independent, since the incoming energy for an interaction is related to the energy deposited at the previous interaction. For each interaction, we randomly sample the incoming energy distribution (except for the first interaction for which we assume the incoming energy is 511 keV). If $L(CS_1, \sigma) < \epsilon$ where ϵ is a predefined threshold, we claim that the sequence is inconsistent and is rejected from the list of possible sequences.

D. Sequencing example for 3 interactions

Fig. 3 gives an example for 3 interactions in the same 511 keV cluster. A photon event with three hits has six possible interaction sequences. In this example, the partial likelihood computed on the first Compton interaction allows one to reject sequences 312 and 213. The examination of the second Compton interaction for the four remaining sequences

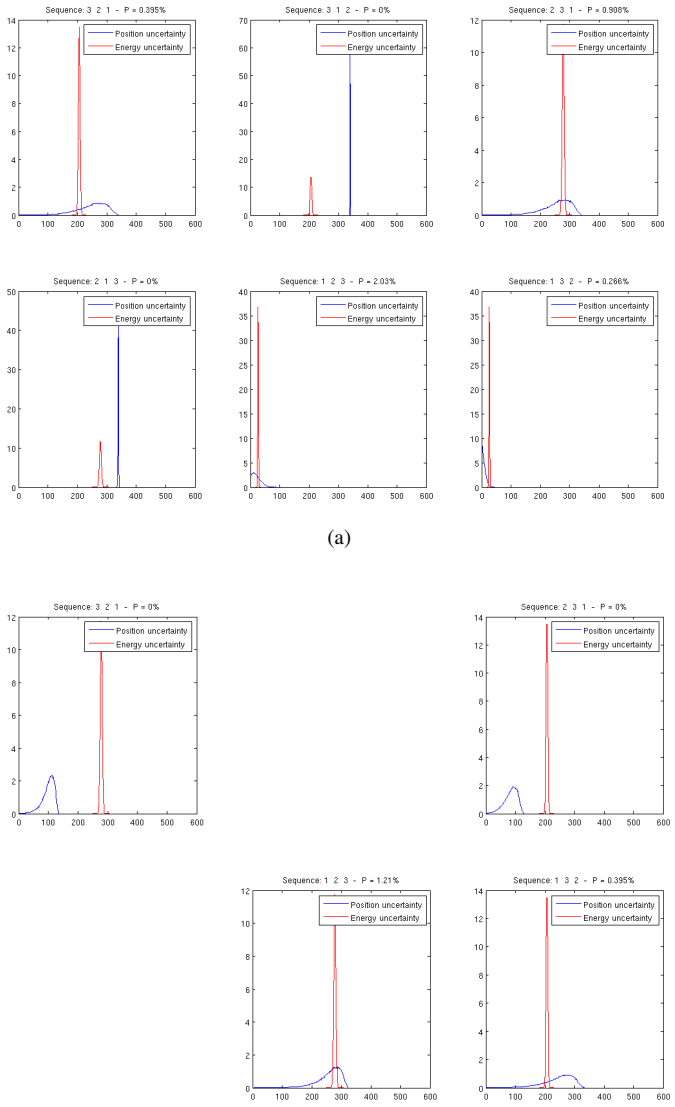

Fig. 3. Example of a 3-interactions problem. For this problem, there are 6 possible sequences. (a) The first Compton interaction consistency is examined. Sequences 312 and 213 are judged impossible. (b) The second Compton interaction is studied for the remaining four sequences. Interactions 321 and 231 are found impossible. For the remaining two sequences, the full likelihood is computed and sequence 123 (the actual correct sequence) is found most likely.

shows that sequences 321 and 231 are also impossible. For the two remaining sequences (123 and 132), the full likelihood is computed using (3). The true sequence 123 is found to be most likely.

III. Results

A. Comparison of the basic positioning algorithms

Two evaluations were performed. A needle beam source of 511 keV photons centered on the edge of one CZT detector slab near the center of the system was set up in GATE in order to measure the point spread function (PSF) of the detector (Fig. 4). The hits were processed using six different methods, and then histogrammed into crystal bins. No image reconstruction was performed. A resolution phantom made of spheres of size 1, 1.25, 1.5, 1.75 mm with twice the diameter spacing was also simulated to evaluate the performance of each positioning algorithm in terms of final reconstructed spatial resolution and contrast. Fully 3D-OSEM with resolution blurring modeled by 1mm-FWHM Gaussian tube-of-response was used to reconstruct the images (Fig. 5). The peak-to-valley ratio was measured on the reconstructed images (Tab. I) for the 1.75 mm spheres. In both simulations, positron range and photon acolinearities were not included.

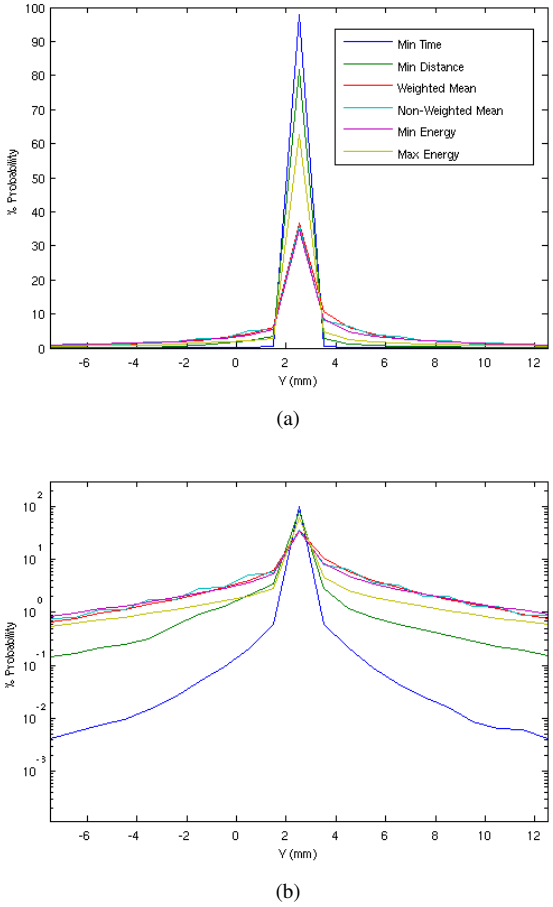

Fig. 4. Point spread function for the six positioning algorithms. Events were generated by simulating a needle beam directed at the edge of one CZT detector within the system depicted n Fig. 1(a). The PSF was obtained by histogramming the estimated position.

B. Evaluation of the maximum-likelihood estimation technique

For the more complex ML technique, we looked at the success rate for both the first interaction and the full sequence. Consistent with the design of our pre-clinical PET system, simulations assumed a 3% energy resolution at 511 keV and a $1 * 1 * 5mm^3$ detector voxel size. Under these conditions, we simulated a beam source normal to the detector face. We evaluated the algorithm on events with 2, 3 and 4 interactions.

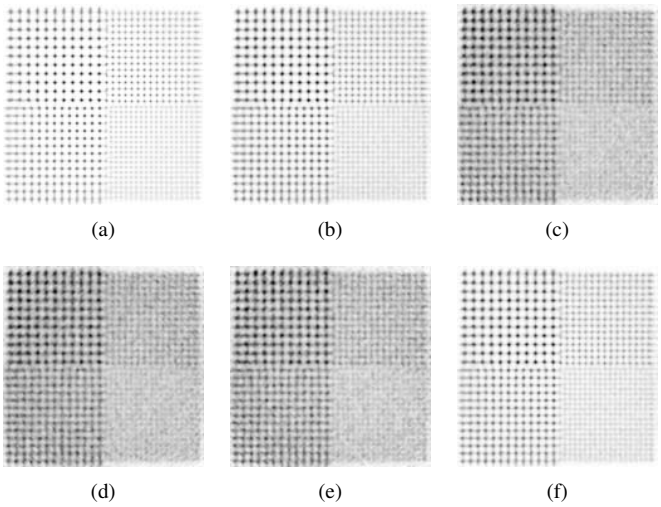

Fig. 5. Spheres phantom (1mm, 1.25, 1.5, 1.75) processed with 6 positioning algorithms ((a) Min Time, (b) Min Distance, (c) Weighted Mean, (d) Non-Weighted Mean, (e) Min Energy and (f) Max Energy) and reconstructed with list-mode 3D-OSEM, 20 updates.

TABLE I

SUCCESS RATE FOR FULL SEQUENCE AND FIRST INTERACTION ESTIMATION

Positioning	**Peak-to-Valley Ratio**	**Standard Deviation**
Min Time	134.7	75.5
Min Distance	21.0	4.9
Weighted Mean	3.4	0.4
Non-Weighted Mean	2.8	0.3
Min Energy	3.3	0.4
Max Energy	3.4	2.4

In each case, 100 events were selected and processed using the algorithm. The small number of events considered was dictated by processing time constraints. The center of mass of the other coincident photon pair was used to estimate the incoming direction of the photon. Table II summarize the success rate of the ML algorithm for recovering the full sequence or the first interaction.

TABLE II

PEAK-TO-VALLEY RATIO FOR THE SPHERES PHANTOM

	PE	**1 CS+PE**	**2 CS+PE**	**3 CS+PE**	**Global**
Full seq.	100%	82%	78%	69%	84.3%
1^{st} inter.	100%	82%	84%	83%	87.3%

The success rate is highly dependent on the performance of the system, namely the spatial and the energy resolution. We therefore studied how the success rate changed when the depth resolution was increased to 1mm and when the energy resolution was either degraded down to 12% FWHM or improved to 0% (perfect energy resolution). Table III summarize the dependency of the algorithm on system performance. Note that even at low energy resolution (12%), the algorithm is still performing better than the minimum distance algorithm which does not use any energy information.

TABLE III

DEPENDENCY ON SYSTEM PERFORMANCE

Energy res.	0%	3%	12%	min dist
Full sequence success rate				
1x1x1 mm	95%	86%	66%	N/A
1x1x5 mm	89%	78%	57%	N/A
First interaction success rate				
1x1x1 mm	97%	90%	77%	69%
1x1x5 mm	90%	84%	71%	68%

IV. DISCUSSION

This approach also makes it feasible to incorporate an *a priori* model of the physical processes in the detector and formulate a Bayesian prior-based maximization. The ML approach assumes all sequences as likely and under this assumption finds the sequence that best agrees with the measurements of energy at each detector. In reality, all sequences are a priori not as likely due to two effect: the exponential attenuation and the non-isotropic distribution of the scatter angle. Indeed, sequences in which the photon travels shorter distances and scatter at lower angles are more likely. The Bayesian problem can be formulated as

$$max\left\{\sigma \mapsto P(E_m = E_c(S)|S = \sigma) * P(S = \sigma)\right\} \qquad (4)$$

where $P(S = \sigma)$ is computed from the exponential attenuation law and the Klein-Nishina differential cross-section formula.

Thorought this work we assumed the energy resolution for our system is $3\% * \sqrt{511/E}$. This is a very conservative estimate since we have observed energy resolution as good as 1.5 % for CZT. However, this model is over-simplified since for low energy interactions the contribution of the readout noise (on the order of 5-6 keV) gets significant. A better energy blurring model will be investigated.

V. CONCLUSION

Because 77.4% of the events for the CZT high-resolution system include two or more interactions, a large number of events are mispositioned if conventional positioning techniques are used. Mispositioned events result in an increase in the tails of the PSF of the detectors, which in turn causes degradations of the contrast and the resolution in images. Accurately estimating which interaction occurred first for each incoming photon event allows to effectively correct for the effects of inter-crystal scatter, a significant image degrading effect for high-resolution PET. While using energy alone is insufficient to select the first interaction, using spatial information results in a significant improvement of the PSF, especially for the minimum distance algorithm (+120% events within the peak for the minimum distance algorithm compared to weighted mean - Fig. 4).

Combining both position and energy to retrace the sequence of interactions that have deposited the spatio-energy pattern observed results in further improvements. This can be achieved by a maximum likelihood approach that computes the likelihood of all possible sequence combination using Compton kinematics. Further evaluation of this technique, as well as incorporation of prior physical models will be investigated.

REFERENCES

[1] C. S. Levin and J. L. Matteson, "Promising characteristics and performance of cadmium zinc telluride detectors for positron emission tomography," *Abstract # M2-117, Book of Abstracts, IEEE NPSS*, p. 136, 2004.

[2] J. R. Stickel and S. R. Cherry, "High-resolution pet detector design: modelling components of intrinsic spatial resolution," *Phys. Med. Bio.*, vol. 50, no. 2, pp. 179–195, Jan 2005.

[3] G. Chinn, A. M. K. Foudray, and C. S. Levin, "Pet image reconstrction with a bayesian projector for multi-electronic collimation schemes." *IEEE Nuclear Science Symposium and Medical Imaging Conference Record.*

[4] A. M. K. Foudray, G. Chinn, C. S. Levin, and P. D. Olcott, "Investigating positioning and scatter rejection algorithms in a high resolution pet system capable of depth of interaction measurement," *Soc Nucl Med annual meeting*, 2004.